IEA 29th TLM Meeting in Leuven (2-5 Sept. '07)
1.5F Spray and Combustion in Diesel Engine

Large Eddy Simulation of Diesel Spray Flame with Eddy-Dissipation Model and CIP Method by Use of KIVALES

H. Gen Fujimoto, T. Hori and J. Senda
Doshisha University
hfujimot@doshisha.ac.jp

ABSTRACT

Three-dimensional large eddy simulation (LES) has been conducted for a diesel spray flame using KIVALES which is LES version of KIVA code. To suppress the numerical instability on the combustible flow as alternative of QSOU and IDC which are KIVA original schemes, CIP method was incorporated into KIVALES in which the spray models are improved and optimized in the earlier studies. Combustion is simulated using the Eddy-Dissipation model. The formation of soot and NO was simulated using Hiroyasu model and KIVA original model, respectively. Three different grid resolutions were used to examine the effect of grid size on the LES spray analysis. Furthermore, the five LES computations on the same condition are performed to examine the cyclic variability of the diesel spray flame. The result shows that the LES approach with 0.5 mm grid size is able to predict unsteady behavior of diesel spray with the three dimensional spray structure and vortical structure. Moreover, in LES approach, the spray flame shape and the spatial temperature distribution are different at each calculation, since the turbulent vortex predicted by LES approach changes at each computation

INTRODUCTION

In diesel engines, fuel is directly injected into the combustion chamber filled with hot and compressed air. The atomizing droplets and fuel vapor are transported and mixed by the turbulent vortex. Thus, the heterogeneous structure denoting the spatial heterogeneous distribution of fuel vapor and temperature is yielded in the diesel spray. The formation of soot and NOx depend on the fuel concentration and temperature in the heterogeneous structure of diesel sprays. Consequently, to improve the prediction of the diesel engine, the prediction of heterogeneous structure is important in addition to the improvement of spray models and introduction of detailed chemistry [1-3]. However, the conventional diesel spray simulations using Reynolds-averaged Navier Stokes (RANS) approach, which is applied in KIVA code, do not represent the heterogeneous structure in diesel sprays. RANS approach is primarily useful for the calculation of large-scale stationary flow structures, while detailed small-scale turbulence eddies are filtered out in the averaging process. It is difficult for RANS approach to simulate the heterogeneous structure in diesel sprays.

Recently, Large Eddy Simulation (LES) approach has been very popular in the industrial machine simulations [4-15] as an alternative way of RANS. In LES, the large energy-containing motion caused by the large eddies is simulated directly, while the effect of small scale fluctuations inside a computational grid is modeled. Thus, LES is able to simulate the larger turbulent vortex than the computational grid size, and predict unsteady characteristics of turbulent flow field. As a result, in LES the formation of nitrogen dioxide and soot in diesel sprays would be captured more accurately, compared to conventional RANS approach.

In earlier studies, the authors have performed the LES analysis of a non-evaporative and an evaporative diesel spray in non-reacting conditions using KIVALES [11-13] which is LES version of KIVA code [14,15]. In KIVALES code, breakup process is modeled using modified TAB model, and interpolated-donor cell differencing scheme [16] is used as the convection scheme. The computational results are found that RANS approach with KIVA indicates a symmetric spray shape in both non-evaporative and evaporative spray simulations. In contrast, the LES analysis with KIVALES achieves the predictions of instantaneous diesel spray structure, such as axi-symmetric shape, intermittency at the spray periphery. Furthermore a good agreement is obtained between LES and experimental results in terms of spray characteristics, such as spray shape, spray tip penetration, sauter mean diameter and liquid length. In addition, to show the difference of the turbulent flow field between RANS and LES, turbulent vortices are visualized with the iso-surface of laplacian pressure. The results show that in LES analysis the turbulent vortices with hairpin like vortices are resolved, and the fuel droplets are dispersed with turbulent vortices.

The objective of this work is to develop LES approach for diesel spray flame using KIVALES. As in the early studies [14-15], k-Δ model, modified TAB model and KIVA original evaporation model are employed for Sub Grid Scale (SGS) stress model, breakup model and evaporation model, respectively. To avoid the numerical instability on the combustible flow, CIP (Cubic-Interpolated Pseudo-Particle Scheme method) is incorporated into KIVALES to calculate convective terms. KIVA original model based on Eddy-Dissipation model is used as the combustion model. The detailed chemistry is not used in order to be simplicity and reduce the computational time and computational memory. The prediction of soot and nitrogen dioxides is performed using the Hiroyasu model and KIVA original model, respectively. First, the grid dependency on the LES of the diesel spray flame is evaluated under three different grid resolutions where grid sizes are 2.0mm, 1.0mm and 0.5mm. Second, the LES results with the grid size of 0.5mm is compared to the experimental result as to the temporal change in the three dimensional spray shape, vortex structure and the combustion product distribution at cross section of the spray. Finally, in order to evaluate the cyclic variability the five LES computations are performed with changing the use of the pseudo-random number at each calculation.

NUMERICAL APPROACH

The CFD code for LES simulations used in this study is KIVALES where LES is incorporated to KIVA (KIVA-3V res.2). It is documented in detail by Sone et al. [11-13].

LES governing equation

Filtering the system of conservation equations for compressible flow yields the equations for LES. The filter used in this study is a top-hat filter, which is suitable for finite volume differencing as in the KIVA code, and as is usual for the simulations of compressible turbulence, we employ Favre-filtering. The equations for LES are:

$$\frac{\partial \bar{\rho}}{\partial t}+\frac{\partial \bar{\rho}\tilde{u}_j}{\partial t}=\overline{\dot{\rho}^s}\,, \tag{1}$$

$$\frac{\partial \bar{\rho}\tilde{u}_i}{\partial t}+\frac{\partial}{\partial x_j}\left(\bar{\rho}\tilde{u}_i\tilde{u}_j-\bar{\tau}_{ij}+\tau_{ij}^{sgs}\right)=\overline{F_i^s}\,, \tag{2}$$

$$\frac{\partial \bar{\rho}\tilde{e}}{\partial t}+\frac{\partial \bar{\rho}\tilde{u}_j\tilde{e}}{\partial x_j}=-\bar{p}\frac{\partial \tilde{u}_j}{\partial x_j}-\frac{\partial h_j^{sgs}}{\partial x_j}-\frac{\partial \bar{q}_j}{\partial x_j}+\bar{\sigma}_{ij}\frac{\partial \tilde{u}_j}{\partial x_j}+\Theta^{sgs}+\Pi^{sgs}+\overline{\dot{Q}^s}+\overline{\dot{Q}^c}\,, \tag{3}$$

$$\frac{\partial \bar{\rho}\tilde{Y}_m}{\partial t}+\frac{\partial}{\partial x_j}\left(\bar{\rho}\tilde{u}_j\tilde{Y}_m-\bar{\rho}\bar{D}_m\frac{\partial \tilde{Y}_m}{\partial x_j}+\Phi_{j,m}^{sgs}+\theta_{j,m}^{sgs}\right)=\overline{\dot{\rho}_m^s}+\overline{\dot{\rho}_m^c}\,, \tag{4}$$

where $\bar{\tau}_{ij}=-\bar{p}\delta_{ij}+\bar{\sigma}_{ij}=-\bar{p}\delta_{ij}+2\bar{\mu}\tilde{S}_{ij}+\lambda\tilde{S}_{kk}\delta_{ij}$, and $\bar{q}_j=-\kappa\,\partial T/\partial x-\rho\sum\tilde{h}_m D_m\left(\partial Y_m/\partial x_j\right)$. Spray terms (superscript s) and combustion terms (superscript c) follow the original models in KIVA code [16]. In these equations, the subgrid stress tensor τ_{ij}^{sgs}, subgrid heat flux h_{ij}^{sgs}, subgrid viscous work Θ_{ij}^{sgs}, subgrid velocity-pressure gradient correlation Π_{ij}^{sgs} and subgrid species mass flux Φ_{ij}^{sgs} all require closure.

SGS model of LES

The subgrid stress tensor τ_{ij}^{sgs} is modeled using the eddy viscosity:

$$\tau^{sgs}=2\bar{\rho}\upsilon_t\left(\tilde{S}_{ij}-\frac{1}{3}\tilde{S}_{kk}\delta_{ij}\right)+\frac{2}{3}\bar{\rho}k^{sgs}\delta_{ij}\,, \tag{5}$$

where ν_t is subgrid eddy viscosity which is modeled with k-Δ model using grid length $\bar{\Delta}$ and subgrid turbulent kinetic energy k^{sgs}. The subgrid eddy viscosity is given by,

$$\upsilon_t=C_\upsilon k^{sgs1/2}/\bar{\Delta}\,, \tag{6}$$

$$\bar{\Delta}=V_{cell}{}^{1/3}\,, \tag{7}$$

where V_{cell} is the computational cell volume.

The subgrid kinetic energy k^{sgs} is obtained by solving the following equation:

$$\frac{\partial \bar{\rho}k^{sgs}}{\partial t}+\frac{\partial \bar{\rho}\tilde{u}_j k^{sgs}}{\partial x_j}=-\tau_{ij}^{sgs}\frac{\partial \tilde{u}_i}{\partial x_j}-D^{sgs}+\frac{\partial}{\partial x_j}\left(\bar{\rho}\frac{\upsilon_t}{Pr_t}\frac{\partial k^{sgs}}{\partial x_j}\right)+\dot{W}^S\,, \tag{8}$$

$$\text{where}\quad D^{sgs}=\frac{C_\varepsilon\bar{\rho}k^{sgs3/2}}{\bar{\Delta}}\,. \tag{9}$$

D^{sgs} is the subgrid kinetic energy dissipation rate. C_ν, and C_ε are the experimental constant. Pr_t denotes the turbulent Prandtl number. In this study, C_ν =0.067 and C_ε =0.916 are chosen [17]. The source term $\dot{W}^s$ is the subgrid turbulent energy production or depletion due to droplet-gas interaction.

The species mass flux Φ_{ij}^{sgs} is modeled by a gradient diffusion closure,

$$\Phi_{i,m}^{sgs}=-\bar{\rho}\frac{\nu_t}{Sc_t}\frac{\partial\widetilde{Y_m}}{\partial x_i}\,. \tag{10}$$

In this study, Liner Eddy Mixing (LEM) model [11] is not employed, since it requires a long time to simulate diesel sprays, compared to gradient diffusion model. The subgrid heat flux h_{ij}^{sgs} is modeled as,

$$h_j^{sgs}=-\bar{\rho}\frac{\nu_t C_p}{\mathrm{Pr}_t}\frac{\partial \tilde{T}}{\partial x_j}\,. \tag{11}$$

The subgrid viscous work Θ_{ij}^{sgs} is modeled as,

$$\Theta^{sgs}=D^{sgs}=\frac{C_\varepsilon\bar{\rho}k^{sgs3/2}}{\bar{\Delta}}\,. \tag{12}$$

The subgrid velocity-pressure gradient correlation term Π_{ij}^{sgs} is ignored.

Calculation of convective term

In LES, it is necessary to apply the computational method with high accuracy for solving the governing equation, since the turbulent vortices which are larger than the grid size are calculated directly [18]. In particular, in the case of the combustible flow, the computational method for the convective terms affect on the accuracy and the stability of the simulation.

In the previous study, the authers used the Interpolated Donor Cell (IDC) differencing scheme to calculate convective terms for LES approach [14-15], because the highly diffusible flow field is obtained in the case of Quasi-Second Order Upwind (QSOU) scheme which is used in the standard KIVA and KIVALES. However, IDC scheme has the high numerical instability so that it is difficult to simulate the diesel spray combustion. Recently, Essentially Non-Oscillatory (ENO) scheme [19] and Weighted ENO (WENO) [20] scheme are proposed to calculate convective schemes with high accuracy. However, in these schemes physical values on a few grid points are necessary to calculate the numerical flux (ex: five grid points). Furthermore, to calculate with high order accuracy the spatial accuracy scheme with the high order accuracy is not set, but also temporal accuracy is high order accuracy, which is second order scheme at least. In KIVA code the temporal accuracy is first-order, and numerical flux is estimated with two points. In this study, CIP scheme [21] is incorporated into KIVALES to calculate convective terms. In this method the numerical flux is estimated with two grid points, and the enough accuracy is obtained if temporal scheme is first-order like KIVA code. CIP scheme is found to give a very stable and accurate results compared to IDC, whereas the computational memory used increases to preserve the information of the slope between the grids in addition to the physical value on the grid.

The one-dimensional convective equation of CIP is explained as follows. In CIP, in addition to the physical value *f*, the spatial derivative of *f*, *g*, is also convection at the same time.

$$\frac{\partial f}{\partial t}+u\frac{\partial f}{\partial x}=0, \tag{13}$$

$$\frac{\partial g}{\partial t}+u\frac{\partial g}{\partial x}=-\frac{\partial u}{\partial x}g, \tag{14}$$

where *u* and *t* are the velocity and time, respectively. If both *f* and *g* are given at two grid points, the profile between these points can be interpolated by a cubic polynominal,

$$F_i(x)=a_i(x-x_i)+b_i(x-x_i)+c_i(x-x_i)+d_i, \tag{15}$$

$$F_i(x_i)=d_i=f_i, \tag{16}$$

$$\frac{dF_i(x_i)}{dx}=c_i=g_i, \tag{17}$$

$$a_i=\frac{g_i+g_{iup}}{\Delta x_i^2}+\frac{2(f_i-f_{iup})}{\Delta x_i^3}, \tag{18}$$

$$b_i=\frac{3(f_{iup}-f_i)}{\Delta x_i^2}-\frac{2g_i+g_{iup}}{\Delta x_i}, \tag{19}$$

$$\Delta x_i=x_{iup}-x_i, \tag{20}$$

$$iup=i-\mathrm{sgn}(u_i), \tag{21}$$

where sgn(u) stands for the sign of *u*. Thus, the profile at the (n+1)th step is readily obtained by shifting the profile by u_i and Δt, so that $f_i^{n+1}=F_i^{n+1}(x_i-u_i\Delta t)$ and $g_i^{n+1}=dF_i^{n+1}(x_i-u_i\Delta t)/dt$; then,

$$f_i^{n+1}=F(x-u\Delta x)=a_i\xi^3+b_i\xi^2+c_i\xi+f_i^n, \tag{22}$$

$$g_i^{n+1}=\frac{dF}{dx}(x-u\Delta x)=3a_i\xi^2+2b_i\xi+g_i^n, \tag{23}$$

where we define $\xi=-u\Delta t$.

Chemical reaction

The chemical reaction is simulated using the original model in KIVA code [16]. A chemical system reacting through *m* reaction is given as follows,

$$\sum_m a_{mr}x_m \rightleftarrows \sum_m b_{mr}x_m \tag{24}$$

where x_m is a symbol for species *m*, a_{mr} and b_{mr} are the integral stoichiometric coefficients for reaction *r*. The chemical reactions are divided into two classes: kinetic reactions and equilibrium reactions.

Kinetic reactions

Kinetic reaction *r* proceeds at a rate $\dot{\omega}_{r,k}$ given by,

$$\dot{\omega}_{r,k}=k_{fr}\prod_m(\rho_m/W_m)^{a'_{mr}}-k_{br}\prod_m(\rho_m/W_m)^{b'_{mr}}, \tag{25}$$

where k_{fr} and k_{br} are the coefficient of forward and back reaction, respectively. W_m is the molecular weight of species *m*. Here the reaction orders a'_{mr} and b'_{mr} is not equal to am_r and bm_r so that a'_{mr} and b'_{mr} are determined empirically [16].

The k_{fr} and k_{br} are given to be of a generalized Arrhenius forms:

$$k_{fr} = A_{fr} T^{\zeta fr} \exp\left(-\frac{E_{fr}}{T}\right), \tag{26}$$

$$k_{br} = A_{br} T^{\zeta br} \exp\left(-\frac{E_{br}}{T}\right), \tag{27}$$

where E_{fr} and E_{br} are activation temperatures of forward and back reaction, and ξ_{fr} and ξ_{br} are the temperature component of forward and back reaction, respectively.

In this study, 4 kinetic reactions is considered according to KIVA manual [22],

$$2C_{12}H_{26}+37O_2 \rightarrow 24CO_2+26H_2O, \tag{28}$$

$$O_2+2N_2 \rightleftarrows 2N+2NO, \tag{29}$$

$$2O_2+N_2 \rightleftarrows NO+N, \tag{30}$$

$$N_2+2OH \rightleftarrows 2H+2NO. \tag{31}$$

The reaction of (28) is the one step reaction of n-dodecane used as the fuel for diesel spray simulation in this study. The formation of NO is described by the reaction of (29)-(31). The kinetic reactions are activated when the gas temperature is higher than 800 K. The coefficient of kinetic reactions are listed in Table 1.

Table 1 Coefficient for kinematics reactions

Kinematics reaction	A_{fr} [cgs units]	A_{br} [cgs units]	E_{fr} [K]	E_{br} [K]	ξ_{fr} [-]	ξ_{br} [-]
$2C_{12}H_{26}+37O_2=24CO_2+26H_2O$	4.5000×10^{11}	0.0	1.5780×10^{4}	0.0	0.0	0.0
$O_2+2N_2=2N+2NO$	1.5587×10^{14}	7.5000×10^{12}	6.4627×10^{4}	0.0	0.0	0.0
$2O_2+N_2=2O+2NO$	2.6484×10^{10}	1.6000×10^{9}	5.9418×10^{4}	1.9678×10^{4}	1.0	1.0

Equilibrium reactions

The rates of equilibrium reactions are implicitly determined by the constraint conditions,

$$\prod_m \left(\rho_m / W_m\right)^{b_{mr}-a_{mr}} = K_r^c(T), \tag{32}$$

where the concentration equilibrium constant $K_r^c(T)$ is assumed to be of the form,

$$K_r^c = \exp\left\{A_r \ln T_A + B_r/T_A + C_r + D_r T_A + E_r T_A^2\right\}, \tag{33}$$

where we define T_A=T/1000. A_r, B_r, C_r, D_r and E_r are the experimental constants.

The six equilibrium reactions are considered according to KIVA example file denoting "itape5.ex1" [22].

$$H_2=2H, \tag{34}$$

$$O_2=2O, \tag{35}$$

$$N_2=2N, \tag{36}$$

$$O_2+H_2=2OH, \tag{37}$$

$$O_2+2H_2O=4OH, \tag{38}$$

$$O_2+2CO=2CO_2. \tag{39}$$

It is assumed that the equilibrium reactions are occurred if the temperature is higher than 1200 K. The model constants in the equation (33) are listed in Table 2.

Table 2 Coefficient in the equilibrium reactions

Equilibrium reaction	A_r	B_r	C_r	D_r	E_r
$H_2=2H$	0.990207	-51.7916	0.993074	-0.343428	0.0111668
$O_2=2O$	0.431310	-59.6554	3.503350	-0.340016	0.0158715
$N_2=2N$	0.794709	-113.2080	3.168370	-0.443814	0.0269699
$O_2+H_2=2OH$	-0.652939	-9.8232	3.930330	0.163490	-0.0142865
$O_2+2H_2O=4OH$	1.158882	-76.8472	8.532155	-0.868320	0.0463471
$O_2+2CO=2CO_2$	0.980875	68.4453	-10.5938	0.574260	-0.0414570

Eddy Dissipation model

In this study, when authors calculate the reaction (28), Eddy Dissipation model [23] is used to represent the interaction between the turbulent flow and chemical reactions. Eddy Dissipation model assumes that the mixing rate of fuel and oxygen is proportional to the ratio D^{sgs} / k^{sgs} where k^{sgs} is the SGS turbulent energy, D^{sgs} is the SGS dissipation rate of k^{sgs}. Thus, the progress rate of equation (28) $\dot{\omega}_{1,ED}$ is given by,

$$\dot{\omega}_{1,ED} = \min\left[\dot{\omega}_{1,k} \quad , \quad A_{ED}\,\rho \min\left(Y_{fuel}, \frac{Y_{O_2}}{r}, \frac{B_{ED} Y_{product}}{1+r} \right) \frac{D^{sgs}}{k^{sgs}} \right], \tag{40}$$

where $\dot{\omega}_{1,k}$ is the progress rate determined by equation (25). Y_{fuel}, Y_{O2} and $Y_{product}$ are the mass fraction of fuel, oxygen and combustion products respectively, A_{ED} and B_{ED} are the experimental constants, and A_{ED} = 18.0 and B_{ED} =0.5 are used in this study. ρ and r are the density and the stoichiometric oxygen to fuel mass ratio, respectively. D^{sgs} are given by the equation (9).

Soot model

Hiroyasu model is incorporated into KIVALES as soot model [24]. This model is semi-phenomenological model, and the production and oxidation are modeled. In Hiroyasu model the soot formation rate is expressed using the following equation,

$$\frac{dm_s}{dt} = \frac{dm_{s,f}}{dt} - \frac{dm_{s,ox}}{dt}, \tag{41}$$

where m_s is the mass fraction of soot, the terms of left hand side represents the soot formation rate. The first and second term of right hand side are the soot production rate and soot oxidation rate, respectively. The soot production and oxidation rate are given using following equations,

$$\frac{dm_{s,f}}{dt} = A_f m_{f,v} p^{0.5} \exp\left(-\frac{E_{s,f}}{RT} \right), \tag{42}$$

$$\frac{dm_{s,ox}}{dt} = A_{ox} m_s \frac{p_{o_2}}{p} p^{1.8} \exp\left(-\frac{E_{s,ox}}{RT} \right), \tag{43}$$

where m_f and m_s denote the mass fraction of fuel vapor and soot, respectively. p_{O2} represents the partial pressure of oxygen and R is the gas constant. Here A_f=150 and A_{ox}=3500 are the experimental constant, and $E_{s,f}$=12500 cal/mol and $E_{s,ox}$=14000 cal/mol denote the activation energy [25].

Computational detail

In this study, we used modified TAB model as breakup model, where the experimental constant K of 8/9 and degree of freedom in chi-square distribution ϕ of 6 are used as well as the earlier study [14,15]. As droplet evaporation model, the KIVA original model is used, which is assumed that the temperature distribution within the fuel droplet is uniform.

Rigid sphere model is employed for the droplet drag model [16]. The effect of droplet distortion on the droplet drag is not taken into account in this study:

$$C_D = \begin{cases} \dfrac{24}{Re_d}\left(1 + 1/6\, Re_d^{2/3}\right) & R_d < 1000 \\ 0.424 & R_d > 1000 \end{cases}, \tag{44}$$

where C_D and Red are the coefficient of droplet drag and the droplet Reynolds number, respectively. The velocity interpolation model proposed by Nordin [26] is employed in order to reduce the grid dependency of spray simulation. The model constant n of 2 is employed. The effect of which SGS velocity in the gas phase affects on the fuel droplet is ignored. The collision and coalescence in the diesel spray are not considered. The computational method used in the present study is listed in table 3.

Table 3 Computational methods

SGS stress model	k-Δ model
Velocity interpolation	Nordin model (n=2)
Droplet drag model	Rigid droplet
Breakup model	Modified TAB (ϕ=6, K=8/9)
Evaporation model	KIVA original
Collision and coalescence	none
Ignition model	none
Combustion model	Eddy-Dissipation model
NOx model	KIVA original
Soot model	Hiroyasu model
Convective scheme	CIP scheme

Computational domain and initial condition

The computational domain is shown in Figure 1. Rectangular computational domain is 30 mm in length and width and 100 mm in height. For the comparison purpose, three different grid resolutions are used as shown in Table 4; coarse grid, standard grid and fine grid. In the fine grid case, there are 60 cells in depth and width direction and 200 cells in height direction. The number of total cells is 720000, and the grid size is 0.5 mm, which is 2.5 times the size of the nozzle diameter d_n= 0.2 mm used in the present study. The computational memory of 2.96 GB is required in the fine grid simulation. In this study, we tried the additional calculation with finer grid where the grid size is 0.25mm. However in this calculation the stiffness is occurred due to the too small grid size. Hence, the most fine mesh case is "fine grid" in this study.

All boundaries of the computational domain are set as the wall. Non-slip conditions are applied. The initial flow condition of the computational domain is the quiescent gas at the desired pressure and temperature. The injection point is set on the top surface of the computational domain. The fuel is injected in the condition of the fuel droplet where the diameter is equaled to the nozzle diameter. The number of fuel parcels injected is 40,000. The profile of the injection velocity is constant, because in the experiment by means of the momentum method the injection rate profile shows approximately constant. The spray cone angle is set as 12 degree, and the injection direction is determined using pseudo-random number, implementing the cone angle of 12 degree. Table 5 denotes the computational conditions. This condition is the same as

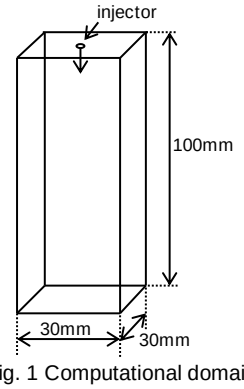

Fig. 1 Computational domain

Table 4 Computational grid

Grid name	Grid size [mm]	The number of grid (Length x Width x Height)	Computational memory [GB]
Coarse grid	2.0	15 x 15 x 50	0.137
Standard grid	1.0	30 x 30 x 100	0.484
Fine grid	0.5	60 x 60 x 200	2.96

Table 5 Computational conditions

Hole diameter	[mm]	0.20
Injection pressure	[MPa]	70
Injection duration	[ms]	2.2
Fuel	[-]	C12H26
Fuel amount	[mg]	20.0
Fuel temperature	[K]	300
Ambient gas oxygen concentration	[-]	21 vol.%
Ambient pressure	[MPa]	4.1
Ambient temperature	[K]	900

the experimental conditions used for the comparison of LES results.

RESULTS AND DISCUSSION

Effect of computational grid size on diesel spray flame simulation

In LES accurate results are obtained with increasing grid resolution, since the dependency of SGS model decreases and the solution is close to the DNS result. In this section, LES of the diesel spray flames under different grid sizes are performed to examine the effect of computational grid size on LES analysis. The LES results are compared to the experimental result as to instantaneous spray shapes and the heat release rate.

Instantaneous spray shape

Figure 2 shows the sectional distribution of the gas temperature at t = 2.2 ms, which is corresponding to the end of the injection. For the comparison purpose, the experimental image taken by shadowgraph method is also shown in this figure. It becomes obvious that temperature distributions and the spray shape in LES analysis are quite different in each grid size. In particular, the spray shape is different from the experimental result in the case of the coarse grid, and unrealistic high temperature region is recognized near the nozzle, since the computational grid size is too large to resolve the turbulent vortex on the computational grid. In contrast, the spray shapes with fine and standard grid are predicted well compared to the coarse grid case. This is because the smaller turbulent vortex in the turbulent flow is captured with increasing the grid resolution.

Heat release rate

Figure 3 shows the comparison of predicted heat release rate under three different grid sizes. The experimental result of heat release rate is also shown. The results show that the prediction of the ignition delay do not depend on the grid size, but the prediction of heat release rates in premixed combustion and mixing control phase strongly depends on the grid size. Course grid case with the grid size of 2.0 mm overpredicts the peak of the heat release rate in the premixed phase compared to the experimental result. In the standard grid case, the peak value and the fluctuation of heat release rate decrease compared to the coarse grid case, while the time of peak heat release is retarded. In fine grid case, the time of peak heat release is middle between the coarse and the standard case, and the peak value of the heat release rate is comparable to the standard case.

The grid dependency is understood as follows. When the spray parcel is evaporated, KIVALES assume that the fuel vapor from the spray parcel diffuses with an infinity speed in the computational cell staying the spray parcel. This means that the assumption error for the infinity diffusion is larger in the LES simulation with the coarser grid resolution. Thus, in the coarse grid case, the too diffusive fuel vapor is simulated compared to the LES results of finer grid case, the combustible fuel-air mixture generated in the ignition delay time is burned rapidly so that the combustion in the premixed combustion phase is overestimated. The difference of ignition delay time between the experimental result and LES results would be improved if authors consider the low-temperature oxidation using Shell model or detailed chemistry.

On the other hand, when authors simulate diesel spray flame in even the fine grid case, the significant difference of the heat release rate is obtained compared to experimental results. Furthermore, the LES results do not converge in the

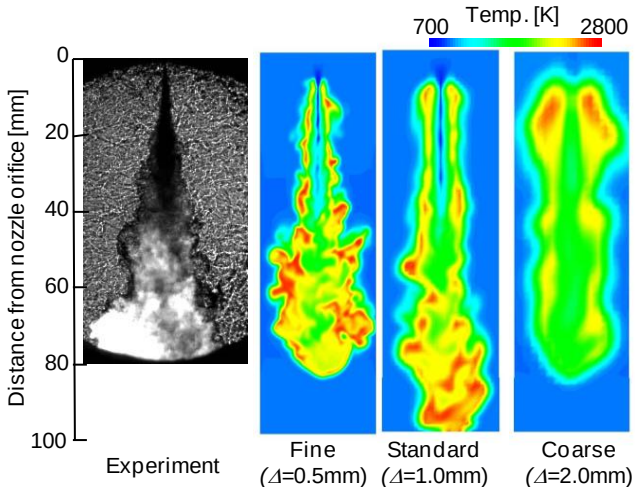

Fig. 2 Effects of computational grid size on instantaneous spray image at 2.2ms. LES images indicate the instantaneous temperature distribution at cross section. (Δ: grid size)

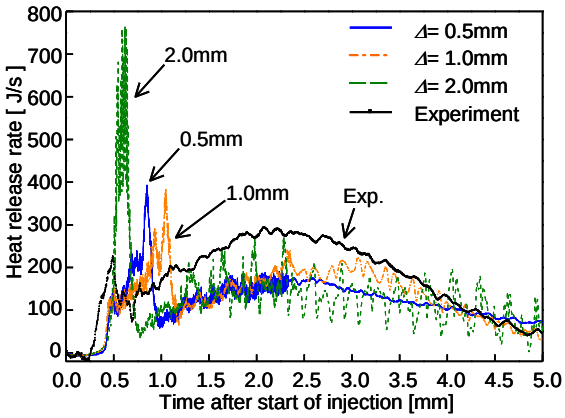

Fig. 3 Comparison of heat release rate in each grid case

computational grid sizes used in this study. Hence, the additional grid refinement should be performed, but as already mentioned, the computation with finer grid is not terminated, because time step is changed to too small value by auto time step control in KIVA code [16]. Consequently, the grid size of 0.5mm would be a standard size for LES approach using KIVALES. In the following section, LES results of the fine grid case are examined.

Temporal change in spray structure using fine grid

The experimental images taken by shadowgraph method and the sectional temperature predicted by LES are shown in Fig. 4 to present the temporal change in the spray structure. In the experimental image the ignition is occurred at 0.2 ms as shown in figure 3. The ignition point is located in the middle of the spray tip penetration. In the premixed combustion phase (t =0.2-0.7 [ms]), the premixed flame enveloped the spray whole region. In the mixing-control phase (t=0.7-2.2 [ms]) the blackbody radiation from soot is recognized as white region in the downstream region of the spray images.

It has been found that in LES the unsteady behavior of diesel spray flame is captured well, since LES approach is able to predict unsteady behavior of turbulent flow with turbulent vortex. The ignition is occurred at 0.4 ms, and the ignition site is located near the nozzle outlet. The premixed combustion flame propagates to the downstream region in the premixed combustion phase (t=0.4-1.0ms). At the end of the premixed combustion phase, the high temperature region is generated at the periphery of the diesel spray. In particular, it is seen that the high temperature region is appeared in the spray tip region at 1.0ms. In the mixing-control phase (t=1.0ms-), this high temperature region in the spray tip at 1.0ms move to the radial direction due to the turbulent mixing. At the end of injection (t≅ 2.2ms), it is seen that the area in spray side becomes the higher temperature than the spray tip region. After the end of the injection (t>2.2ms), the meandering motion is simulated in the upstream region of the spray due to the turbulent vortices.

Instantaneous structure of diesel spray flame

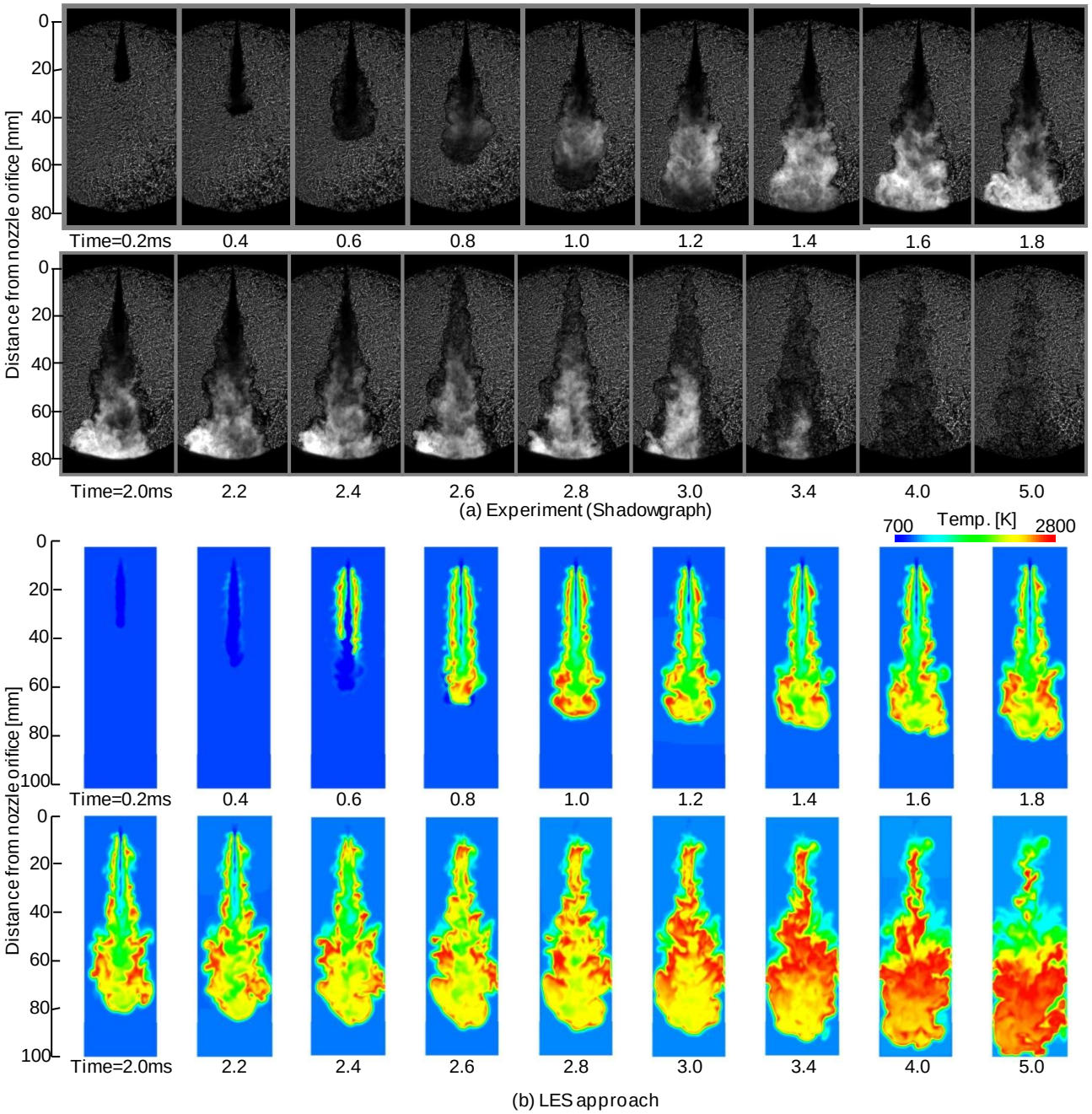

Fig. 4 Temporal change in the spray shape. (upper: experiment, lower: sectional value of temperature)

The three-dimensional structure of the diesel spray flame, turbulent vortices and the spray sectional value simulated at 2.2 ms are displayed in Fig. 5. In the visualization of the three-dimensional spray flame, the definition of the spray is the region indicating above the mass fraction of 0.01. The visualization of the three-dimensional diesel spray flame is done using the volume rendering. The color in the spray flame indicates the gas phase temperature. The second invariant of the deformation tensor is used to identify the turbulent vortices in the diesel spray. The positive area of the second invariant of the deformation tensor indicates the vortex tube in the high vorticity region. The sectional value of temperature, OH radical, CO, NO, soot and density are also shown in the figure. OH radical and CO are simulated in the kinetic reaction and the equilibrium reaction. The formation of NO and soot is simulated using KIVA original model and Hiroyasu model, respectively.

As shown in Figure 5, it is found that the three-dimensional structure of diesel flame predicted in the LES approach demonstrates the unsteady behavior with intermittency at the spray periphery. Notice that the visualization of turbulent vortices is found that the hairpin-like structures exist in the diesel flame as shown in the jet [27] and LES of non-evaporative and evaporative diesel spray [14,27]. These vortices enhance the local mixing between fuel and air, temperature, and affect on the local equivalence ratio and local temperature distribution in the diesel spray or the heterogeneous structure.

In the sectional image, OH radical is formed at the spray periphery which is corresponding to the high temperature region. CO and NO are also generated in the high temperature region. It is notice that the distribution of these species is transformed due to the vortices in the turbulent flow. However, the soot predicted indicates in only the nozzle region. As experimental results, the high concentrate region of soot is the tip of the spray. The soot model parameter optimization or the soot model based on the detailed chemistry mechanisms is needed to capture the soot production and oxidation process.

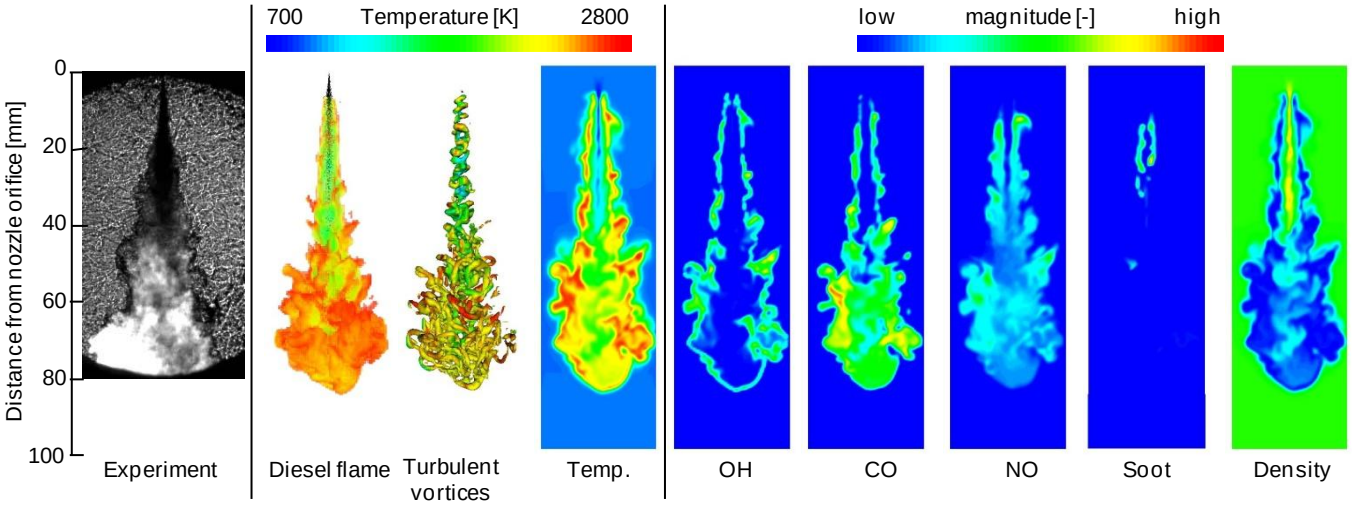

Fig. 5 Comparison of Instantaneous spray structure at 2.2ms between LES results and the experimental result.

Cyclic variability at each injection

One of the advantages on LES over RANS is that the valiance can be obtained in addition to the statistical value. In the engines simulation, LES is expected to simulate the cyclic variability as simulating the multi-cycle. In this section, the cyclic variability at each injection is evaluated by the results of five computations with the fine grid.

The computational results are, however, quite the same at five computations, if the peso-random number used in KIVALES is quite the same. In present study, the difference at each diesel spray flame is expressed to change the peso-random number, which means that the each traveling direction of injected spray parcels is changed within the some injection angle in each computation. It is noticed that the injection velocity profile and injection amount are the same in

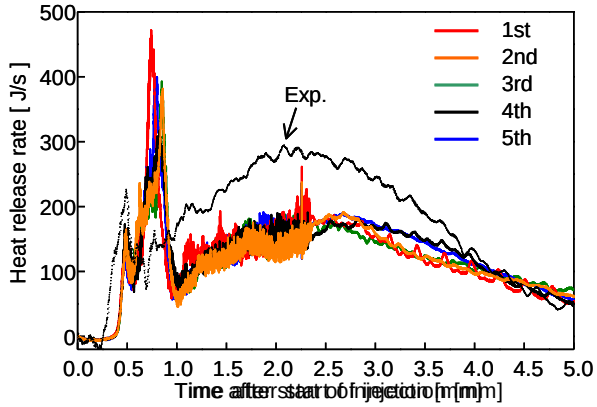

Fig. 6 Variability on heat release rate of five simulations.

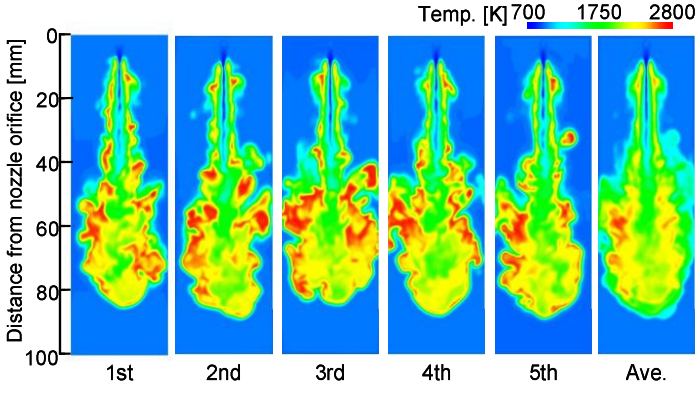

Fig. 7 Sectional temperature distribution of five computations and ensemble averaged one. “Ave.” denotes the ensemble averaged value of five computations. (LES results with fine grid, t=2.2ms).

each simulation.

Heat release rates at five calculations are shown in Fig.6. The experimental result which is an ensemble mean value of five experimental results is also shown in this figure. It is found that the profiles of heat release rates are slightly different at each computation though the poor agreement is obtained between the experimental result and each computation. Fig. 7 is the instantaneous sectional temperature distribution at 2.2 ms. The ensemble mean temperature of five calculations is also shown in this figure. It is found that the instantaneous spray shape and instantaneous spatial temperature distribution are different at each calculation. In contrast, the ensemble averaged temperature image denoting "Ave." demonstrates the symmetric temperature distribution as simulated using RANS approach. This is because the turbulent vortex predicted by LES approach is different at each simulation and the local mixing and transportation is changed in each computation. If we perform five computations with the same procedure using RANS approach (i.e., KIVA), the difference of diesel spray flame in each computation would not be obtained like LES approach, and the difference of each computation in RANS approach is caused by the model of unsteady behavior (i.e., random walk), not just turbulent vortex.

SUMMARY AND CONCLUSION

Three-dimensional large eddy simulation of the diesel spray flame is performed using KIVALES, which is LES version of KIVA code. Eddy-Dissipation model is used as combustion model to estimate the interaction between turbulent flow and chemical reaction. CIP method is incorporated into KIVALES due to the reduction of the numerical instability on the combustible flow. The formation of NO and soot are simulated using KIVA original model and Hiroyasu model.

First, to examine the effect of the computational grid size on LES of diesel spray flames, diesel spray simulations are performed under three different grid sizes of 2.0mm, 1.0mm and 0.5mm. The following results are obtained;

(1) LES results strongly depend on the grid size. The 2.0mm grid case shows the unrealistic temperature distribution is predicted at cross section. On the other hand, the grid size of 0.5mm is desirable to simulate the diesel spray flame, since the unsteady vortex of diesel spray flame is well captured. The computational result with the grid size of 0.5mm is, however, quite different from the experimental result in terms of the heat release rate and LES results do not converge in the grid size range used in this study. The additional grid refinement is needed to examine the grid sensitivity of LES.

(2) The LES results of 0.5mm grid size capture the temporal change in the three dimensional structure and unsteady behavior of the diesel spray combustion. The turbulent vortices with hairpin like vortices are captured as well as the computation of a jet, the non-evaporative and the evaporative diesel spray in earlier studies. The distribution of NO, CO, OH at the cross section shows the unsteady behavior due to the transportation of the vortices in the turbulent flow. the soot distribution predicted by Hiroyasu model is, however, underestimated in the spray tip region.

Secondly, the five LES computations are performed with changing the use of the pseudo-random number at each calculation in order to evaluate the cyclic variability

(3) It is found that each computation is different as to temperature distribution at cross section and the heat release rates, since the turbulent vortex predicted by LES approach is changed in each computation. In contrast, the ensemble averaged temperature at cross section indicate the symmetric distribution along spray axis as predicted in RANS approach.

ACKNOWLEDGMENTS

The authors would like to appreciate Tomoki Ikeda and Sho Sakurai (Graduate student of Doshisha University) for providing many suggestions or experimental results. And the work were carried out in the Energy Conversion Research Center of Doshisha University which has been supported by Academic Frontier' Project for Private Universities: matching fund subsidy from The Ministry of Education, Culture, Sports, Science and Technology, 2003-2007. A part of this work was supported by Grant-in-Aid for Scientific Research (C), No. 18560213, of Japan Society for the Promotion of Science.

REFERENCES

(1) R.D.Reitz and Diwakar, "Structure of High-Pressure Fuel Sprays", SAE paper 870598, pp1-18 (1987).
(2) Kawano, D., Senda, J., Wada, Y., Fujimoto, H.,Goto, Y., Odaka, M., Ishii, H. and Suzuki, H., "Numerical Simulation of Multicomponent Fuel Spray", SAE paper 2003-01-1838, 2003.
(3) Ito, T., "The clarification of the particle production mechanism on the unsteady spray combustion" (in Japanese), Ph D thesis, Doshisha University, 2004.
(4) Ken Naitho et al., "Large Eddy Simulation of Premixed-Flame in Engine based on the Multi-Level Formulation and Renormalization Group Theory", SAE paper (920590), pp.1-16 (1992).
(5) I Celik et al., "Large eddy simulations of in-cylinder turbulence for internal combustion engines: a review", Int. J. Engine Research 2, 2, pp.119-148 (2001).
(6) Daniel Lee, Eric Pomraning, Christopher J. Rutland, LES Modeling of Diesel Engines, SAE technical paper, 2002-01-2779, pp.1-13, 2002.
(7) S. V. Apte, M. Gorokhovski, P.Moin, LES of atomizing spray with stochastic modeling of secondary breakup, Int. J. Multiphase Flow, Vol 29, pp.1503-1522, 2003.
(8) Kimura,S., Kosaka, H., Himeno, R. and Matsui,Y., A Numerical Simulation of Turbulent Mixing in Transient Spray by LES (Comparison Between Numerical and Experimental Results of Transient Particle Laden Jets), SAE Paper No.2004-01-2014, (2004).

(9) Bing Hu and Christopher J. Rutland, Flamelet Modeling with LES for Diesel Engine Simulations, SAE paper 2006-01-0058, pp.1-10, 2006.
(10) Rahul Jhavar and Christopher J. Rutland, Using Large Eddy Simulations to Study Mixing Effects in Early Injection Diesel Engine Combustion, SAE paper 2006-01-0871, pp.1-14, 2006.
(11) K. Sone, S. Menon, Effect of Subgrid Modeling on the In-Cylinder Unsteady Mixing Process in a Direct Injection Engine, J. Eng. Gas Turb. Power, Vol. 125, pp. 435-443, 2003.
(12) Sone, K., Patel, N. V., and Menon, S., KIVALES: Large-Eddy Simulations of Internal Combustion Engines. Part I: Theory and Formulation, Technical Report CCL-00-008, Georgia Institute of Technology, 2000, http://www.ccl.gatech.edu/home_html.
(13) Sone, K., Patel, N. V., and Menon, S., KIVALES: Large-Eddy Simulations of Internal Combustion Engines. Part Ⅱ: KIVALES User's Manual, Technical Report CCL-00-009, Georgia Institute of Technology, 2000. http://www.ccl.gatech.edu/home_html.
(14) Hori, T., Kuge, T., Senda, J. and H. Gen Fujimoto, "Large Eddy Simulation of Diesel Spray Structure in Constant Volume Vessel by Use of KIVALES", ICLASS2006 in CD-ROM, 2006.
(15) Hori, T., Senda, J., Kuge T. and H. Gen Fujimoto, "Large Eddy Simulation of Evaporative Diesel Spray in Constant Volume Vessel by Use of KIVALES", SAE Powertrain & Fluid Systems Conference and Exhibition, SAE paper 2006-01-3334, 2006.
(16) Amsden, O'Rourke, KIVA-Ⅱ: A Computer Program for Chemically Reactive Flows with Sprays, LA-11560-MS, Los Alamous National Laboratory, 1989.
(17) Menon S., Subgrid Combustion Modelling for Large-Eddy Simulations, Int. J. Engine Res., Vol.1, No.2, pp.209-227, 2000.
(18) Pope, Turbulent Flows, Cambridge Univ. Press, Cambridge, UK, 2000.
(19) A. Harten, B. Engquist, S. Osher and S. J. Chakravarthy, Uniformly high order essentially non-oscillatory schemes, J. Comut. Phys. Vol.71, No.231, 1987 .
(20) G.-S. Jiang and C.-W. Shu, Efficient implementation of weighted ENO schemes, J. Comput. Phys. Vol.126, No.202, 1996.
(21) Takewaki, H., Nishiguchi, A. and Yabe, T., The Cubic-Interpolated Pseudo-Particle (CIP) Method for Solving Hyperbolic-Type Equations, J. Computer Physics, 61, pp.261-268, 1985.
(22) Amsden, "KIVA-3: A KIVA Program with Block-Structured Mesh for Complex Geometries", LA-12503-MS, Los Alamous National Laboratory (1993).
(23) Magnussen, B. F., and Hjertager, B. H., On Mathematical Modeling of Turbulent Combustion with Special Emphasis on Soot Formation and Combustion, 16th Symposium (Int.) on Combustion, The Combustion Institute, pp. 719-729, 1977.
(24) Hiroyasu, H., Kadota, T., Arai, M., Development and Use of a Spray Combustion Model to Predict Diesel Engine Efficiency and Pollutant Emissions. Part 1: Combustion Modeling, Bull JSME, Vol.26, No.214, pp.569-575,1983.
(25) M. A. Patterson, S.-C. Kong, G.J. Hampson, and R. D. Reitz, Modeling the Effects of Fuel Injection Characteristics on Diesel Engine Soot and NOx Emissions, SAE paper 940523, pp.1-17, 1994.
(26) Niklas Nordin, "The KIVA JumpStation", http://www.tfd.chalmers.se/~nordin/KJS/.
(27) Sudo, J., Matsubara, K., Kobayashi, M. Watanabe, H., and Matsudaira, Y., Coherent Structures in a Fully Developed Stage of a Non-isothermal Round Jet, JSME B Vol.69, No.681, pp.1200-1207, (2003).

NONMENCLATURE

CIP	Cubic-Interpolated Pseudo-Particle Scheme method
ED	Eddy-Dissipation
IDC	Interpolated donor cell differencing scheme
LES	Large Eddy Simulation
LEM	Liner Eddy Model
QSOU	Quasi-Second Order Upwind scheme
RANS	Reynolds Averaged Navier Storks
SGS	Sub Grid Scale
am_r	integral stoichiometric coefficient
A	pre-exponential factor
A_r	the model constant in the equilibrium reaction
A_{ED}	The experimental constant in ED model
b_{mr}	integral stoichiometric coefficient
b_r	back reaction
B_{ED}	The experimental constant in ED model
B_r	the model constant in the equilibrium reaction
C_r	the model constant in the equilibrium reaction
CD	coefficient of droplet drag
C_ε	experimental constant
C_ν	experimental constant
d	droplet
D_m	molecular diffusivity of species m
D_r	the model constant in the equilibrium reaction
D^{sgs}	subgrid scale kinetic energy dissipation rate
e	specific internal energy
E	activation energy
E_r	the model constant in the equilibrium reaction
f	physical value
f_r	forward reaction
g	gas or spatial derivative of f in CIP
h	heat flux
h^{sgs}	sub grid scale heat flux
h_m	the specific enthalpy of species m
K_r^c	the concentration equilibrium constant
k^{sgs}	turbulent kinetic energy
K	the ratio of the total energy in distortion and oscillation to the energy used in TAB model
k_{fr}	the coefficient of forward reaction
k_{br}	the coefficient of back reaction
m_f	mass fraction of fuel vapor used in soot model
m_s	mass fraction of soot

n	parameter in velocity interpolation
p	pressure
p_{O2}	partial pressure of oxygen
Pr_t	turbulent Prantl number
r	droplet radius or the stoichiometric oxygen to fuel mass ratio
$\dot{Q}^c$	The chemical heat release term in the energy equation
$\dot{Q}^s$	The source term due to the spray interaction
Re	Reynolds number
Re_d	Reynolds number for a droplet
sgs	subgrid scale
S_{ij}	rate of strain tensor
Sc_t	turbulent Schmidt number
t	time
T	temperature
u	gas velocity
V_{cell}	Volume of computational cell
W_m	molecular weight
$\dot{W}^s$	subgrid turbulent enegy production or depletion
x_m	one mole of species m
Y_{fuel}	mass fraction of fuel
Y_m	mass fraction of species m
Y_{O2}	mass fraction of oxygen
$Y_{products}$	mass fraction of combustion products
δ_{ij}	kronecker delta
ϕ	the degree of freedom in chi-distribution
Φ^{sgs}	sub grid scale species mass flux
κ	thermal conductivity
λ	the second coefficient of viscosity
μ	viscosity
ν_t	eddy viscosity
Π^{sgs}	sub grid scale velocity-pressure gradient correlation
Θ^{sgs}	sub grid scale viscous work
ρ	density
σ	surface tension
σ_{ij}	viscous stress tensor
τ_{ij}	stress tensor
τ^{sgs}	sub grid scale stress tensor
$\bar{\Delta}$	grid size
Δt	time step
$\tilde{\bullet}$	filter
$\bar{\bullet}$	density-weighted filter
$\dot{\omega}_{r,k}$	progress rate of kinetetic reaction r
$\dot{\omega}_{r,ED}$	progress rate calculated by ED model
ζ	temperature component